Renewable and Sustainable Energy Reviews 110 (2019) 174–187

Contents lists available at ScienceDirect

Renewable and Sustainable Energy Reviews

journal homepage: www.elsevier.com/locate/rser

Power-to-fuels via solid-oxide electrolyzer: Operating window and techno-economics

Ligang Wang[a,b,*], Ming Chen[c], Rainer Küngas[d], Tzu-En Lin[e], Stefan Diethelm[a], François Maréchal[b], Jan Van herle[a]

[a] Group of Energy Materials, Swiss Federal Institute of Technology in Lausanne (EPFL), Sion, Switzerland
[b] Industrial Process and Energy Systems Engineering, Swiss Federal Institute of Technology in Lausanne (EPFL), Sion, Switzerland
[c] Department of Energy Conversion and Storage, Technical University of Denmark, Roskilde, Denmark
[d] Haldor Topsøe A/S, Kongens Lyngby, Denmark
[e] Institute of Biomedical Engineering, National Chiao Tung University, Hsinchu, Taiwan, ROC

ARTICLE INFO

Keywords:
Power-to-fuel
Energy storage
Solid-oxide electrolysis
Co-electrolysis
Operating window
Degradation

ABSTRACT

Power-to-fuel systems via solid-oxide electrolysis are promising for storing excess renewable electricity by efficient electrolysis of steam (or co-electrolysis of steam and CO_2) into hydrogen (or syngas), which can be further converted into synthetic fuels with plant-wise thermal integration. Electrolysis stack performance and durability determine the system design, performance, and long-term operating strategy; thus, solid-oxide electrolyzer based power-to-fuels were investigated from the stack to system levels. *At the stack level*, the data from a 6000-h stack testing under laboratory isothermal conditions were used to calibrate a quasi-2D model, which enables to predict practical, isothermal stack performance with reasonable accuracy. Feasible stack operating windows meeting various design specifications (e.g., specific syngas composition) were further generated to support the selection of operating points. *At the system level*, with the chosen similar stack operating points, various power-to-fuel systems, including power-to-hydrogen, power-to-methane, power-to-methanol (dimethyl ether) and power-to-gasoline, were compared techno-economically considering system-level heat integration. Several operating strategies of the stack were compared to address the increase in stack temperature due to degradation. The modeling results show that the system efficiency for producing H_2, methane, methanol/dimethyl ether and gasoline decreases sequentially from 94% (power-to-H_2) to 64% (power-to-gasoline), based on a higher heating value. Co-electrolysis, which allows better heat integration, can improve the efficiency of the systems with less exothermic fuel-synthesis processes (e.g., methanol/dimethyl ether) but offers limited advantages for power-to-methane and power-to-gasoline systems. In a likely future scenario, where the growing amount of electricity from renewable sources results in increasing periods of a negative electricity price, solid oxide electrolyser based power-to-fuel systems are highly suitable for levelling the price fluctuations in an economic way.

1. Introduction

High-temperature electrolysis via solid oxide cells is promising for energy storage and production of synthetic fuels via power-to-x concepts [1]. With solid-oxide electrolyzer (SOE), excess renewable electricity can be efficiently converted to energy carriers such as hydrogen via electrolysis of steam (SE) or synthesis gas (syngas, H_2 + CO) via co-electrolysis (CE) of steam and CO_2. The produced hydrogen or syngas could be further processed to easy-to-store and -distribute synthetic methane (METH) or liquid fuels, particularly, methanol (MeOH), dimethyl ether (DME) and gasoline (GASO). These fuels can be either used in the transportation sector [2–4] or converted back into electricity to address peak demand [5]. Unlike conventional alkaline or proton exchange membrane based low-temperature electrolysis, SOE offers high electrical efficiency, and uniquely allows co-electrolysis of steam and CO_2, and the opportunity of thermal integration with industrial processes, e.g., fuel-synthesis processes.

The SOE technology for producing hydrogen, carbon monoxide, or syngas has developed rapidly in recent years, from material-, cell- and stack-levels [6,7], to system levels on design [8–10], demonstration [11,12] and operation [13], to product and business levels for commercialization [14–16]. Novel or improved material systems to overcome the critical issues of state-of-the-art yttria-stabilized-zirconia (YSZ) - $La_{0.8}Sr_{0.2}MnO_3$ (LSM) system on, e.g., carbon surface

* Corresponding author. Group of Energy Materials, Swiss Federal Institute of Technology in Lausanne (EPFL).
E-mail addresses: lgwangeao@163.com, ligang.wang@epfl.ch (L. Wang).

https://doi.org/10.1016/j.rser.2019.04.071
Received 4 January 2019; Received in revised form 6 April 2019; Accepted 24 April 2019
Available online 02 May 2019

Table 1
List of conditions for characterizing stack performance (*iV* measurements) and long-term durability testing [46].

Measurement type	Temp., °C	Gasses to Ni/YSZ		Oxygen to LSCF/CGO
		Composition	Total flow, sccm/cm^2	Total flow, sccm/cm^2
*iV*1	800	H_2O/H_2 (50/50)	12.44	5.70
*iV*2	800	$CO_2/H_2O/H_2$ (45/45/10)	6.21	2.85
*iV*3	750	$CO_2/H_2O/H_2$ (45/45/10)	6.21	2.85
*iV*4	700	$CO_2/H_2O/H_2$ (45/45/10)	6.21	2.85
*iV*5	750	$CO_2/H_2O/H_2$ (45/45/10)	4.97	2.85
*iV*6	750	$CO_2/H_2O/H_2$ (45/45/10)	9.59	2.85

deposition, contaminant poisoning, have been advanced [17] with continuous fundamental understanding on physical-chemical phenomena in these heterogeneous electrochemical materials at a microstructure level [18–20]. Cells and stacks have been characterized and tested for durability [21] under various conditions (e.g., dynamic renewable-power profile, contaminant type and concentrations), and iteratively improved [22,23] with the aid of different modeling activities [24] to enhance the stacks' robustness, manufacturability, efficiency and cost-viability [25,26]. Steam electrolysis to produce H_2 for various applications, e.g., energy storage [27], biogas upgrading [15,28], urban energy system [29,30] and industrial coupling [31], has been well demonstrated with the development of critical system components, e.g., methanation reactor [32] and thermal-driven oil-free gas re-circulator [33]. Despite these advances, cost reduction and lifespan enhancement are still the major focus to be affordable for wide deployment.

The durability of SOE stacks under steam electrolysis has been investigated by a number of groups, at 650–850 °C and at current densities of up to 0.8 A/cm^2 [34–44]. All these tests were reported below 4000 h, except the following two longest: (1) up to 9000 h test on a Topsoe Fuel Cell 25-cell stack (assembled in 2012) at 750 °C and 0.57–0.72 A/cm^2, showing a degradation of 2%/1000 h (%/kh) [42], and (2) over 10 000 h test on a SOLIDpower 6-cell short stack at below 750 °C and 0.5–0.6 A/cm^2, concluding a degradation rate of below 0.5%/kh [45]. However, the information on the durability of SOE stacks running in CE remains scarce. Recent CE tests reported were based on the stacks from Haldor Topsoe: (1) an over 1000 h test on a 10-cell stack at 800 °C and 0.75 A/cm^2 with no notable degradation after 1000 h [41], and (2) a 6000 h test on a 8-cell stack at 750 °C and 0.25–0.5 A/cm^2 [46], which will be further introduced later.

Critical challenges to cope with stack degradation at the system level may not be identified from existing experience, since most demonstrations are employed for proof-of-concept purpose but not for testing long-term operation. The design and sizing of components, particularly, the heat exchangers of the balance of plant (BoP), are based on initial mass and energy balance. It has not yet been reported how the system efficiency and stack operation changes with degradation.

Importantly, there have been no previous studies which combine long-term stack performance and system modeling to address various issues related to feasible stack operation, design-point selection, techno-economic performance, and long-term operating strategy at the system level of various power-to-fuel systems for producing H_2, METH, MeOH, DME and GASO. More specifically, this study focuses on the following points:

- feasible stack operating maps/windows for both SE and CE to facilitate design-point selection,
- comprehensive and fair comparison of techno-economic performance of power-to-fuels, and
- preliminary investigation of stack/system long-term operating strategy regarding degradation.

The paper is organized as follows: The stack and the experimental conditions are first introduced in section 2. Then, state-of-the-art power-to-fuel systems are described and reviewed with industrial experiences and knowledge, followed with brief information on component and system modeling (section 3.2). Afterwards, the stack-level investigation is performed in section 4.1 to identify the practical operating window of the stack (section 4.1.2). The considered power-to-fuel systems are then evaluated comprehensively with similar stack operating points (section 4.2.1) from technical (section 4.2.2) and economic (section 4.2.3) viewpoints. Subsequently, long-term operating strategies are investigated in section 4.3 to cope with the thermal management issue due to stack degradation. Finally, the conclusions are drawn in section 5.

2. Testing of solid-oxide cell stack

The stack tested was an experimental short stack (Delta-design) produced by Topsoe Fuel Cell with the 2014-design: 8 planar type Ni/yttria stabilized zirconia electrode supported cells. Each cell is composed of a Ni/YSZ support, a Ni/YSZ active fuel electrode, an YSZ electrolyte, and a strontium and cobalt co-doped lanthanum ferrite/gadolinia doped ceria oxygen electrode with a barrier layer at the electrolyte-and-oxygen-electrode interface. The active area of each cell is approximately 87.7 cm^2 with a footprint of 12 × 12 cm^2. Further details about the cells can be found elsewhere [47,48]. The cells were connected by interconnects made of Crofer22APU with a protective coating on both sides, which forms 8 serial repeating units (SRUs).

The stack was reduced at 800 °C, by supplying a mixture of H_2 and N_2 to the Ni/YSZ electrode compartment. Hereafter, the stack performance was characterized by performing DC polarization (*iV*) curves at 800, 750, and 700 °C, with either H_2O/H_2 (50/50) or $CO_2/H_2O/H_2$ (45/45/10) fed to the Ni/YSZ electrode (cathode in the SOE mode) compartment and pure oxygen to the oxygen electrode (anode in SOE mode) compartment. The detailed conditions are listed in Table 1. The following gasses from Air Liquide were used in the study: pure O_2 of industrial grade, ≥ 99.5%; hydrogen, N30, ≥99.9%; CO_2 ≥ 99.7%. The performance of the stack has been discussed in detail in Ref. [46] and is employed for model calibration discussed in section 4.1.1.

It should be noted that a full-sized Delta stack at the time included 50 SRUs. In 2014, Topsoe introduced a next generation stack design, which addresses several issues with the Delta design. The new design, called TSP, includes 75 cells, a larger cell active area, lower degradation rates and improved robustness. Data demonstrating the improved performance and robustness of the TSP stack are available [49,50].

3. SOE-based power-to-fuel systems

3.1. System description and considerations

This paper focuses on the applications of both SE and CE to produce gaseous and liquid fuels, i.e., H_2, METH, MeOH, DME and GASO. The SOE is employed only with oxygen sweep via anode gas recirculation so that pure oxygen can be produced as a by-product. The technical

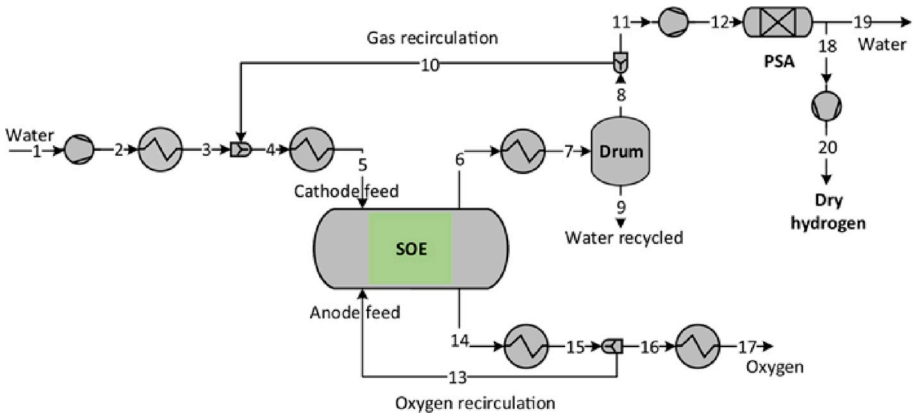

Fig. 1. The power-to-hydrogen system with oxygen as the sweep gas. Heat exchanger network is not explicitly designed but its performance is estimated with classical heat-cascade calculation described elsewhere, e.g., Ref. [52]. The final hydrogen pressure is assumed to be 350 bar.

realization of gas recirculation at both cathode and anode sides is out of the scope of this paper. In addition, CO_2 sources are not considered here, since the energy consumption, the CO_2 purity, type and concentration of contaminants in the CO_2 flow depend on the source of CO_2 and the employed capture technology.

Only the conceptual designs are evaluated to compare and position the considered applications. Therefore, heat exchanger network is not designed in detail, but its performance is estimated with classical heat cascade calculation, as described in section 1 in the supporting information.

3.1.1. Power-to-hydrogen

For power-to-hydrogen (PtH) system (shown in Fig. 1), demineralized water (1) is vaporized and superheated (3) to mix with the cathode recirculation (10) as the reactant feed, which ensures a certain amount of H_2 (usually 10 vol%) in the feed flow to avoid re-oxidation of Ni-YSZ [51]. The fed steam (5) will be electrolyzed up to a conversion of 85–90%, a value to avoid reactant starvation, which may cause cell damages. The outlet gas mixture (6) will be cooled with water knock-out (9). The remaining gas (11) will be compressed and processed usually by a pressure swing adsorption unit (PSA) to obtain fuel-grade dry H_2 (over 99.999 vol%), which is further compressed to 350 bar for light vehicles.

The anode sweep oxygen (13) is fed to the SOE to carry out the produced oxygen and for thermal management purpose. During start-up, the sweep oxygen (13) should come from additional oxygen storage, while during normal operation, it should be recirculated from the anode outlet (15). The remaining oxygen (17) becomes a by-product of the system. Note that the anode gas can also be air, thus avoiding the storage of oxygen.

3.1.2. Power-to-methane

For carbon fuel production, both PtH via SE and power-to-syngas via CE are considered to prepare suitable feedstocks for the fuel-synthesis processes, as illustrated in Fig. 2. For the SE, CO_2 is fed via (18) into the fuel-synthesis subsystem, while for the CE it is fed to the SOE via (20-21-22) by mixing with steam feed (3) and recirculated cathode gas (10). For the CE, the flow rates of CO_2 (20) and steam (1) are adjusted together with the controllable operating variables of the SOE to obtain a gas composition (12) suitable for downstream fuel synthesis.

For the methanation of carbon oxides (200–550 °C, 5–30 bar) [53–55], the active reactions are CO_2 methanation (Eq. (1)), CO methanation (Eq. (2)) and reverse water-gas shift reaction (RWGS, Eq. (3)):

$$CO_{2(g)} + 4\ H_{2(g)} \rightarrow CH_{4(g)} + 2\ H_2O_{(g)},\ \Delta H\ (25\ °C) = -165\ \text{kJ/mol} \quad \text{Eq. 1}$$

$$CO_{(g)} + 3\ H2_{(g)} \rightarrow CH4_{(g)} + H_2O_{(g)},\ \Delta H\ (25\ °C) = -206\ \text{kJ/mol} \quad \text{Eq. 2}$$

$$CO_{2(g)} + H_{2(g)} \rightarrow CO_{(g)} + H_2O_{(g)},\ \Delta H\ (25\ °C) = 41\ \text{kJ/mol} \quad \text{Eq. 3}$$

The limiting factors are the kinetics or chemical equilibrium [54]. Available literature focus mainly on catalysts (e.g., Ni or Ru with Al_2O_3 or TiO_2 supports [56]) and reaction mechanisms (e.g. Refs. [57–60]), on reactor design/operation (e.g. Refs. [61,62]), and on reactor systems (e.g. Refs. [54,63]). Available concepts of catalytic methanators [63] include isothermal or adiabatic fixed-bed, fluidized-bed, or structured reactors. Adiabatic fixed-bed reactors are the most mature with low complexity and high flexibility; however, the peak temperature may reach very high values immediately after the reactions start [32,64], thus limiting the single-pass conversion. Adiabatic fixed-bed reactor systems usually connect 2–5 reactors in series [15,54,63,65] with inter-stage water knock-out. To reduce system complexity and enhance single-pass conversion, isothermal reactor concepts are under investigation [15,61] with various schemes of staged CO_2 feed [54] and cooling [66,67]. It is, however, not possible to use external, jacketed cooling to establish evenly distributed temperature profiles; therefore, internal cooling (e.g., with water [61]) has been employed for more effective heat removal from the reaction zone. Another added value of internal cooling is the direct internal steam generation for the stack, which could also enhance the cooling effect via two-phase flow. Such a direct internal steam-generation scheme is currently experimentally investigated by some of the co-authors to achieve a stable steam supply for the stack. This scheme is the most attractive reactor concept for the SOE-based power-to-methane (PtMETH). The possible thermal coupling and the intrinsic high electrolysis efficiency allows to achieving uniquely high system efficiency of ideally over 80% or even 90% on an HHV basis, depending on the stack operating modes and points [68]. This high system efficiency might not be achieved by using other cooling schemes. Thus, this paper considers the isothermal methanation reactor.

The compact methanation subsystem proposed in Ref. [9] is illustrated in Fig. 2. The hydrogen-rich gas mixture (23) is heated up to 240 °C (25), depending on the catalysts employed, to start the reactions. For steam-electrolysis, H_2 from electrolysis (12) and CO_2 (19) are fed stoichiometrically ($H_2/CO_2 = 4$) into the methanator. For CE, stream (19) is not used, since syngas with the recommended composition (a molar-fraction based ratio $M = (H_2 - CO_2)/(CO + CO_2)$ of 3 [69]) is obtained directly from the stack via (12). The product (26, a gas mixture of H_2, CO, CO_2, CH_4 and H_2O) is then cooled down under the process pressure (4–30 bar) with water knock-out, before entering an

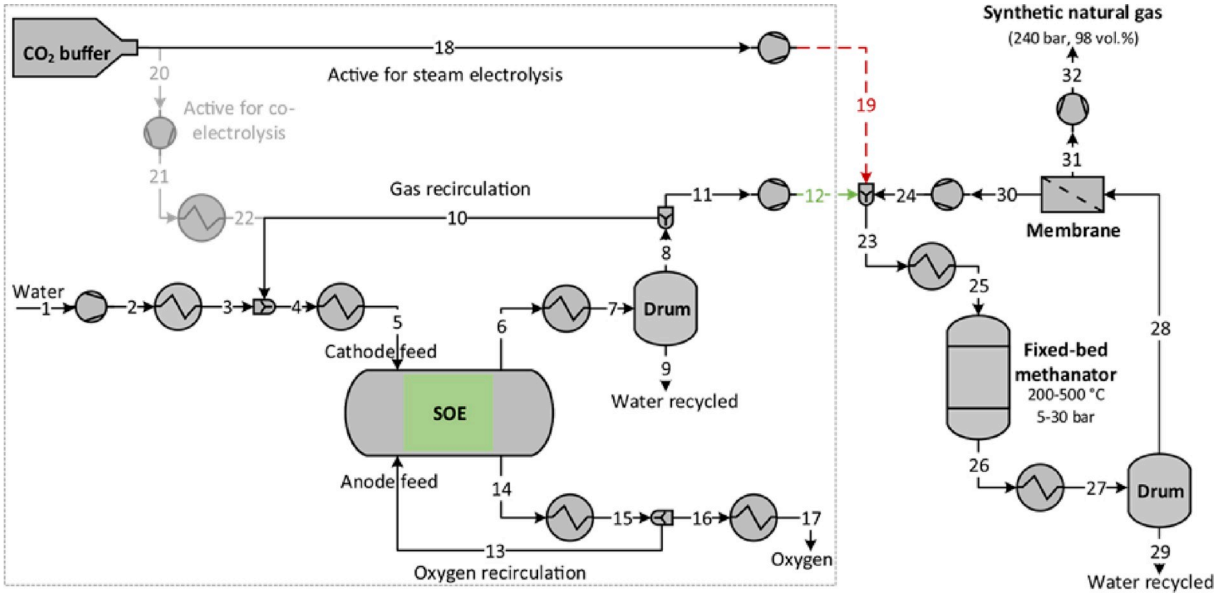

Fig. 2. Schematic of SOE based power-to-methane system with oxygen as the sweep gas (adjusted from Ref. [9]). The membrane module is designed to achieve a methane purity (over 98 vol%) for transportation use. The dashed box is not repeated in Figs. 3, Figs. 4 and 5.

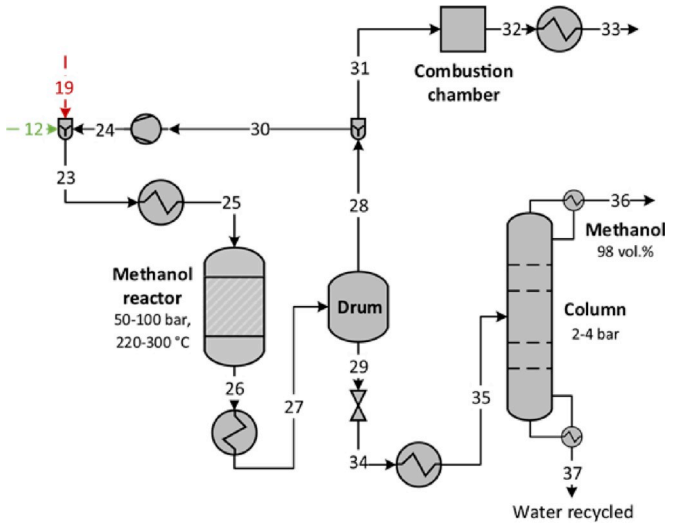

Fig. 3. Schematic of the methanol synthesis process. The hydrogen/syngas production process illustrated in Fig. 2 is not repeated but only the bridging streams 12 and 19 are highlighted. Methanol purity achieved is over 98 vol%.

upgrading module to obtain desired methane purities (e.g., 98 vol% for transportation fuel).

Membrane-based upgrading module is preferred for compact system designs, because of available commercial polymer membranes [70]. Considering cost, selectivity and permeability among various membranes of organic polymers and non-organic materials, the highly-selective polyimide membrane was employed.

3.1.3. Power-to-methanol

MeOH synthesis reaction (220–300 °C, 50–100 bar) is less exothermic than methanation reactions:

$$CO_{2(g)} + 3\,H_{2(g)} \rightarrow CH_3OH_{(g)} + H_2O_{(g)},\ \Delta H(25\,^{\circ}C) = -50\ kJ/mol \quad \text{Eq. 4}$$

$$CO_{(g)} + 2\,H_{2(g)} \rightarrow CH_{(g)}OH_{(g)}, \Delta H\ (25\,^{\circ}C) = -91\ kJ/mol \quad \text{Eq. 5}$$

$$CO_{2(g)} + H_{2(g)} \rightarrow CO_{(g)} + H_2O_{(g)}, \Delta H\ (25\,^{\circ}C) = 41\ kJ/mol \quad \text{Eq. 6}$$

Over 300 °C, the catalysts (e.g., commercial $Cu/ZnO/Al_2O_3$ [71]) may be permanently damaged, due to sintering and fusion [72].

Currently, MeOH is synthesized from syngas, obtained by the steam reforming of methane. Alternatively, MeOH can be produced with the aid of co-electrolysis of CO_2 and H_2O [73]. However, the adaptation to CO_2 feedstock faces new challenges in the development, testing and scale-up of catalysts, as well as the corresponding process design and optimization [74]. Due to slow kinetics compared to the methanation reactor, MeOH synthesis reactor can be adiabatic or isothermal with relatively easy temperature control [75] to ensure a peak temperature below 300 °C [74]. Therefore, the reactor system is rather simple with one adiabatic or shell-and-tube reactor, and with/without gas recirculation [76–80].

The methanolization of carbon oxides follows three stages [81], as shown schematically in Fig. 3. Raw feed gas is first compressed by multi-stage compressors. The gas compositions are for SE (CO_2 methanolization), H_2 (12)/CO_2 (19) = 3, while for CE (syngas methanolization), (H_2 - CO_2)/(CO + CO_2) = 2 by the stream (12). Secondly, the pressurized feed mixture (23) is heated up and reacted for MeOH. Thirdly, the product gas mixture (26) of H_2, CO, CO_2, CH_3OH and H_2O is cooled down to separate the unreacted gas (28) and liquid (29, H_2O and CH_3OH mixture), which is further heated up to 80 °C (35) and purified in a distillation column under near atmospheric pressure (e.g., 2–4 bar) in order to obtain a fuel-grade MeOH (36, over 98 vol%). The unreacted gas (28) is recycled via (30) with a small (1% [80]) flare gas (31) to avoid the accumulation of inert gases. A more detailed MeOH synthesis process can be found elsewhere, e.g., Refs. [79,82–84].

3.1.4. Power-to-DME

DME can be synthesized directly from syngas [85,86], or H_2 and CO_2 [87,88] at 20–50 bar and 200–260 °C with hybrid bifunctional catalysts [89,90] combining $CuO/ZnO/Al_2O_3$ for MeOH synthesis with γAl_2O_3 or (H-)ZSM-5 for MeOH dehydration. Direct DME synthesis is commercially available but less mature in terms of catalyst development and multi-functional reactor design, and therefore, is not considered further here.

The well-known, mature DME synthesis is dehydration of pure MeOH with γ-Al_2O_3 as the catalyst:

$$2\,CH_3OH_{(g)} \rightarrow CH_{(g)}OCH_{3(g)} + H2O(g),\ \Delta H\ (25\,^{\circ}C) = -21\ kJ/mol \quad \text{Eq. 7}$$

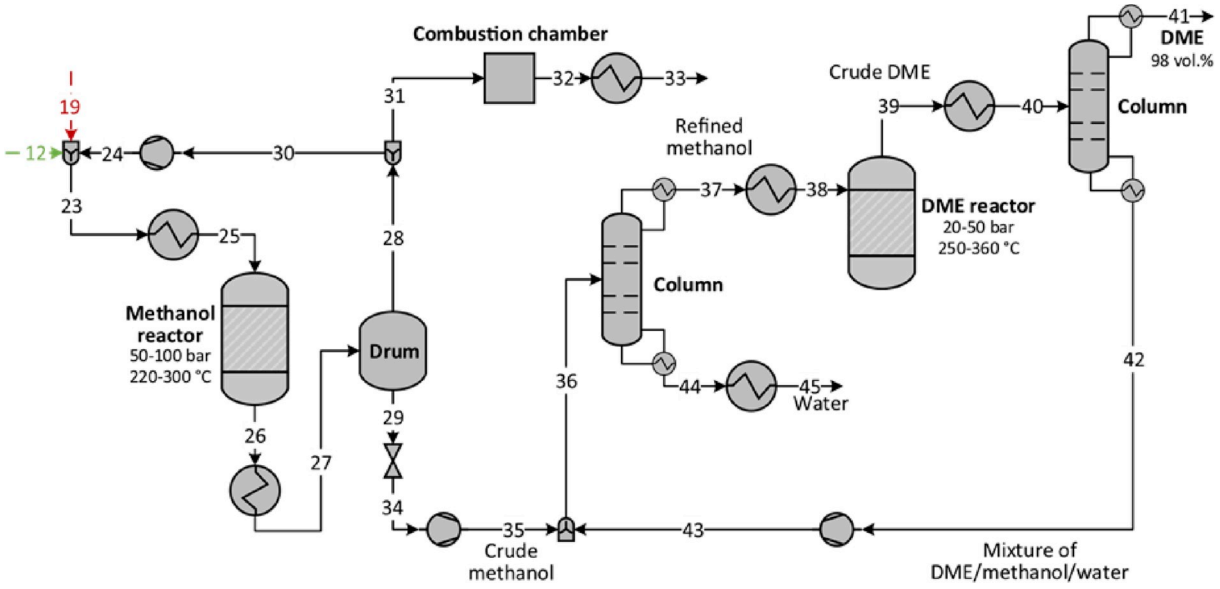

Fig. 4. Schematic of DME synthesis and upgrading from methanol pathway. The hydrogen/syngas production process illustrated in Fig. 2 is not repeated, but only the bridging streams 12 and 19 are highlighted. The DME product purity is expected to be over 98 vol%.

The slightly-exothermic reaction is equilibrium limiting, thus an adiabatic reactor can best handle the synthesis with proper reaction conditions, process and control [91]. The typical reactor inlet temperature is 250–360 °C to achieve per-pass MeOH conversion of 70–85% [74]. The technology providers include Haldor Topsøe, Lurgi, Toyo, MGC and JFE Holdings.

For a first evaluation of SOE based power-to-DME (PtDME), a basic two-stage process of subsequent MeOH synthesis and dehydration is used for indirect DME synthesis as illustrated in Fig. 4. For MeOH synthesis, the recommended composition of feed gases, and reactor conditions have been introduced in section 3.1.3. The crude MeOH (35) is mixed with the recycled DME/MeOH (43) and is separated in a distillation column to obtain high-purity MeOH (37). The subsequent DME reactor performs MeOH dehydration. The mixture of DME/MeOH/H_2O (40) is further separated for DME product (over 98 vol%) and unreacted MeOH is recycled by (42).

3.1.5. Power-to-gasoline

Different routes are available for carrying out power-to-gasoline (PtGASO) conversion. One approach is to produce syngas using SOE as outlined in Fig. 2, and convert the obtained syngas into hydrocarbons using Fischer-Tropsch synthesis [92]. This approach will be used in a demonstration project in Norway, including CO_2 air capture, steam electrolysis using SOE and a Fischer-Tropsch reactor [93]. The project is expected to be starting in 2020 with an annual production of 10 million liters of gasoline and a targeted price of less than 2 €/litre [94].

An alternative route to converting syngas into gasoline is to use MeOH as an intermediate in the MeOH-to-gasoline (MtGASO) process, typically using zeolite catalysts (e.g., ZSM-5). MtGASO first coverts MeOH to DME and then DME to gasoline, which passes through a complex upgrading process. In this paper, only the MtGASO route is considered, since (1) the process for PtGASO can be simply extended from the PtMeOH/DME process, thus making different conceptual power-to-fuel scenarios easily comparable, and (2) combining PtMeOH and MtGASO allows co-production of the two important fuels and even DME.

The formation of hydrocarbons in the MtGASO process is a complex network of numerous reactions, but the most important mechanism is

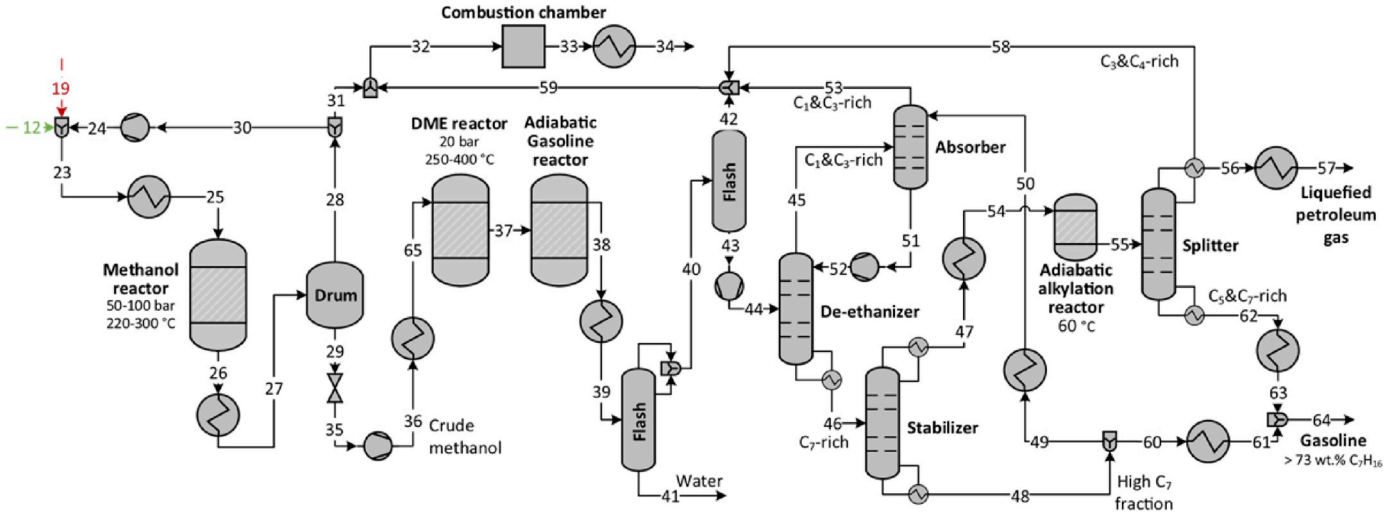

Fig. 5. Schematic of gasoline synthesis and purification from methanol pathway. The hydrogen/syngas production process illustrated in Fig. 2 is not repeated, but only the bridging streams 12 and 19 are highlighted. The major product is gasoline, represented by C_7 chemicals, with liquefied petroleum gas as the by-product.

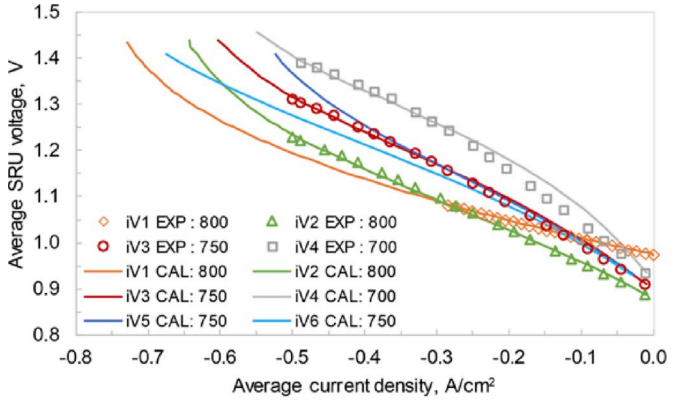

Fig. 6. Comparison between measured and predicted *iV* curves. Scattered symbols are measured *iV* points, while solid lines are the predicted *iV*s. The predictions for *iV*5/6 are given without illustrating the experimental points (see Ref. [46]).

the formation of the monomer [CH_2], which sets the starting point for the polymerization reactions. The [CH_2] monomers then polymerize to longer paraffins, olefins and oxygenated hydrocarbons. The dehydration of MeOH and DME for gasoline occur as follows:

$$n\ CH_3OH \rightarrow n\ [CH_2] + n\ H_2O \quad \text{Eq. 8}$$

$$n\ CH_3OCH_3 \rightarrow n\ 2[CH_2] + n\ H_2O \quad \text{Eq. 9}$$

The overall reaction can be represented by.

$$\text{Oxygenates (MeOH/DME)} \rightarrow C_{1-2} + C_{3-4} + C_5 + C_{>6} + H_2O + \text{Heat} \quad \text{Eq. 10}$$

with C5 as LPG and $C_{>6}$ as gasoline (typically C_7H_{16}). State-of-the-art commercial technology can derive high-quality product, with 85% gasoline and 11–13% liquefied petroleum gas (LPG) of the total product stream [95]. In fact, since the 1980s to cope with the oil crisis, commercial MtGASO processes have been proven by many companies, e.g., Haldor Topsøe A/S, ToyoEngineering Ltd., ExxonMobil Research and Engineering Co, Air Liquide, S.A. or JFE Holding Inc. A large commercial plant employing MtGASO (Topsoe Improved Gasoline Synthesis) to produce 15 500 bbl/day synthetic gasoline [96] will start operation in 2019. Current research activities focus on catalyst development [97–100] and process improvement [101,102].

For the PtGASO to be evaluated, a simplified two-stage gasoline synthesis is considered with gasoline synthesis and upgrading, as illustrated in Fig. 5, following [103]. The MeOH synthesis process is the same as given in Fig. 3. For MtGASO, the obtained crude MeOH (35) is pumped up to 23 bar (36), vaporized and superheated to 297 °C (65), and fed to an adiabatic fixed-bed DME reactor, in which MeOH is converted to an equilibrium mixture of MeOH, DME and H_2O (37). The mixture at 22 bar then enters the gasoline reactor for MeOH and DME dehydration.

For the complex product recovery and upgrade process, the MtGASO effluent (39) is first separated into water (41), crude gasoline (43) and gas streams (42). The condensed crude gasoline (43) then enters product recovery and is fractionated in the de-ethanizer, where the light hydrocarbons C_1-C_3 are separated at the top via (45) to the absorber and the C_7-rich mixture (46) enters the stabilizer. The stabilizer further separates the LPG-rich stream (47) and stabilized gasoline (48), part of which (49) is recycled back to the absorber and the remaining (60) becomes heavy gasoline. The LPG-rich stream (47) passes through the alkylation reactor and then a column to obtain the final LPG (57) as the main by-product by separating the C_4 hydrocarbons out, since too much C_4 hydrocarbons, especially isobutene, can cause the Reid vapor pressure to exceed allowable limits. Finally, the recovered light gasoline (62) is mixed with the heavy gasoline (61) as the major gasoline product (64).

3.2. System modeling

The key components to be modelled for the processes described in section 3.2 are (1) the stack, (2) reactor, (3) distillation column, and (4) heat exchanger network. The stack and process modeling of the stack subsystem has been discussed in detail in Ref. [68]. The reactors are modelled either with chemical equilibrium or semi-empirical data (for gasoline synthesis reactor). All distillation columns are modelled rigorously and heat exchanger network is estimated, for a conceptual design investigation, with mathematically-formulated heat cascade calculation developed and employed elsewhere, e.g., Refs. [52,84,104–106]. More details on the modeling and technology specifications can be found in section 1 of the supporting information.

4. Results and discussion

4.1. Stack operating windows

4.1.1. Model calibration under isothermal conditions

With the model and calibration procedure given in Ref. [68], the SOE model was calibrated considering the average cell performances of the measurements *iV*1/2/3/4 [46] and cell dimensions given in Ref. [107]. The relationships of the measured and calculated current densities of each experimental point, namely the parity plot, are illustrated in Figure S 2. Together with Fig. 6, the predictions agree well with each experimental *iV* curve. Particularly, when the average cell current density becomes large (e.g., over 0.6 A/cm^2) compared to the reactant feed flow rate, the reactant starvation is captured by the mass diffusion equations employed (i.e., dusty gas model). It can be concluded that the calibrated model is satisfactory for the purposes of this paper and the average SRU performance can be aggregated to represent the stack performance.

4.1.2. Operating windows under adiabatic conditions

Practical (adiabatic) performance differs from the isothermal performance presented in the previous section. Only a limited temperature variation was observed during experiments, due to the temperature stabilization by electrical heating for the large heat losses without stack insulation. However, under adiabatic conditions, electrochemical performance and cell temperature are interacted strongly, as shown in Figs. S 3–S 5. Therefore, adiabatic operating maps can be more credible to screen feasible operating points under different operating conditions.

High-resolution initial operating maps for the SOE at 750 °C (inlet temperature) and 1 bar under adiabatic conditions are generated for H_2, METH, MeOH synthesis with or without gas recirculation. The obtained operating maps, simplified in Figs. S 6 – S 10, are visualized as operating windows in Fig. 7 and Figure S 11.

For each operating window, the lower line is constrained by the minimum reactant utilization considered, while the upper line is constrained by one of the factors:

- for large current densities, the maximum allowed temperature,
- for medium current densities, the maximum allowed reactant utilization, and
- for small current densities, the minimum allowed temperature.

When applying large current densities, increasing feed flows cannot provide enough cooling and there is not enough parameter space to adjust the operating variables. When operating at low current densities, the small ohmic heating cannot maintain the stack temperature. Particularly, it is difficult to find initial operating points below 0.2 A/cm^2 at 1 bar and 750 °C (inlet temperature). In the medium range of current density, increasing the current density and feed flows generally enlarge the operating windows, and achieve, at the upper line, the

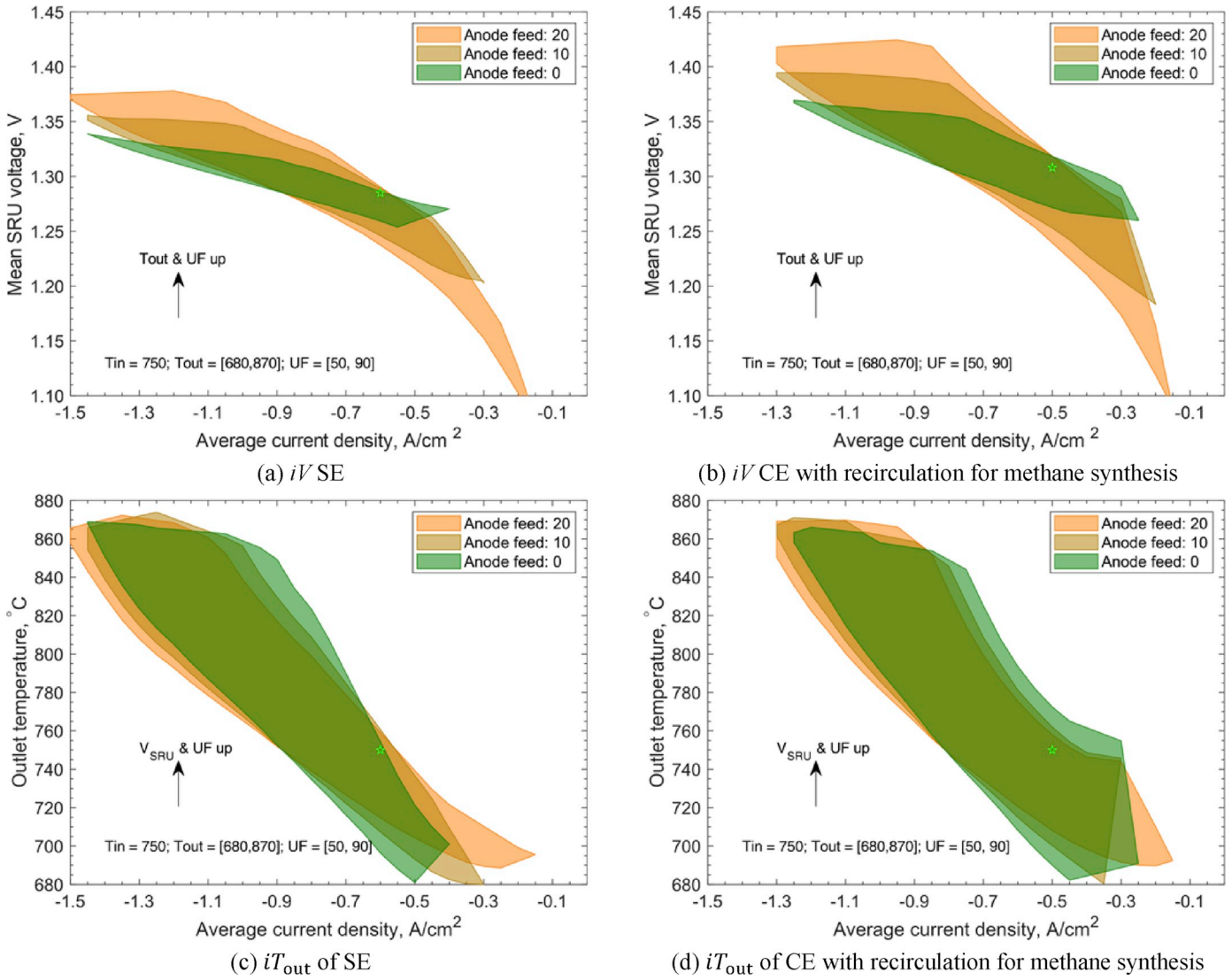

Fig. 7. Initial operating windows of SE (a, c) and CE with syngas production for methane synthesis (b, d). The SOE is operated under adiabatic conditions at atmospheric pressure and an inlet temperature of 750 °C with no heat losses considered. Feasible operating points are selected based on the constraints of the maximum temperature gradient between the inlet and outlet (120 °C), a minimum temperature of 680 °C, a practical reactant-utilization range of 50–90% and 10 vol % H_2 at the cathode feed. Feasible operating points are identified by adjusting the feed flow rates of steam (2–20 sccm/cm^2) and oxygen (0–20 sccm/cm^2). Gas recirculation ratio and CO_2 flow rate are determined to achieve specific syngas modular number and 10 vol% H_2 at the cathode feed. Details of all the operating points have been listed in Figs. S 6 – S 10. The operating maps for methane production without gas recirculation and methanol production are given in Figure S 11. The green stars in these figures are selected as the operating points for the system analysis in section 4.2. (For interpretation of the references to colour in this figure legend, the reader is referred to the Web version of this article.)

practical maximum reactant utilization at a safe stack temperature.

Increasing anode feed flows extends the operating windows at low and high current densities. For example, in Fig. 7 a, there are no feasible initial points below 0.4 A/cm^2 without sweep gas, while with 20 sccm/cm^2 sweep gas the stack can even operate below 0.3 A/cm^2 due to the heat supplied by the sweep gas. A high flow rate of sweep gas allows the stack operation with large operating voltage to ensure that the heat produced internally can be removed to avoid overheating issues. Besides, the cathode gas recirculation is positive for extending the operating windows, particularly for the low and medium current density, and results in a smooth upper line of the windows (Fig. 7 b vs Fig. S 11 a; S 11 c vs e).

The operating *iV* windows of CE (Fig. 7 b and Figure S 11 a, c, e) are broader than those of SE (Fig. 7 a). For CE, it has been identified in Ref. [108] that the electro-chemical reaction is dominated by H_2O electrolysis, and the CO_2 fed into the stack is converted by RWGS (Eq. (3)). At the same current density, CE presents higher voltage due to, e.g., additional mass diffusion resistance, and produces more heat inside the stack than SE. On the contrary, the endothermic RWGS can absorb heat and affect the stack temperature. Therefore, the iT_{out} map depends on the rate of RWGS, which increases with the increase in current density (CO_2 feed fraction): At lower current density, the temperature range of the CE is larger due to relatively low RWGS rate, while at high current density, the stack temperature can still be below the maximum allowed value even with higher voltage.

4.2. Performance of power-to-fuel systems

4.2.1. The selected stack operating points

To evaluate the performance of different PtF systems in a fair and rational way, three similar adiabatic operating points suitable for the downstream fuel synthesis are chosen from the corresponding operating maps identified in section 4.1.2 and listed in Table 2: P1 SE, P2 CE for methane, and P3 CE for MeOH, DME and GASO. The current densities

Table 2
Practical (initial) operating points at 750 °C and atmospheric pressure, with an anode feed flow rate of 2.85 sccm/cm^2 and cathode gas recirculation to have 10 vol% H_2 at the cathode inlet.

	SRU voltage/current density	Dry-gas recirculation	Cathode feed, composition (CO_2/H_2O/H_2/CO/CH_4)	Utilization factor	Outlet temp.	Cathode outlet flow, composition (CO_2/H_2O/H_2/CO/CH_4)	Syngas module number	Anode outlet flow	Cell power
	V	%	sccm/cm^2	%	°C	sccm/cm^2, -	–	sccm/cm^2	W/cell
P1: SE[a]	1.285/0.6	11.5	5.42, 0/90/10/0/0	85.7	750	5.42, 0/13/87/0/0	–	4.94	67.6
P2: CE for METH	1.308/0.5	15.2	4.74, 19/69/10/3/0	80.3	750	4.66, 4/11/67/17/1	3.04	4.59	57.3
P3: CE for MeOH	1.319/0.5	16.7	4.97, 23/63/10/3/0	77.8	750	4.90, 5/12/61/21/1	2.06	4.59	57.8

[a] Under adiabatic conditions, it is not feasible to operate the SOE thermo-neutrally at 0.5 A/cm^2 with an outlet temperature of 750 °C (Fig. 7(a)); otherwise, the reactant utilization will be very high over 90% (Figure S 6), which will be harmful to the SOE lifetime. Therefore, a safe operating point of 0.6 A/cm^2 is selected.

of all selected operating points are set at 0.5 A/cm^2 (with the exception of SE, see note) as often used for durability tests (e.g., Table 1) and demonstration plants. All chosen points are under atmospheric pressure, thus internal methanation will not be promoted. The recirculation of cold cathode gas is 11–17% and the reactant utilization reaches 77 – 86%. The details listed in Table 2 lay the ground to discuss and compare the performance of various power-to-fuel systems in the following sections.

4.2.2. Thermodynamic performance

System-level heat integration is first investigated and compared among different power-to-fuel systems with fixed SOE hardware (150 stacks of 50 × 87.7 cm^2 active area). Then, the difference in system efficiency is further elaborated.

4.2.2.1. System-level heat integration. As shown in Fig. 8, the bottleneck of heat integration is a large amount of heat required for steam generation, in case of no waste heat available from neighboring industrial processes. If heat self-sufficiency cannot be achieved, external hot utilities, e.g., electrical heating, must be used to drive part of the steam generation. For example, electrical heating is always necessary for PtH, although the compression heat, if properly valorized, can contribute 1/4 of the total heat required by the steam generation (Fig. 8 a).

Heat released from exothermic fuel synthesis processes can improve the overall heat integration and reduce hot-utility consumption, particularly, when combining with CE. For producing the same amount of fuels (current density applied), CE needs less steam fed into the stack, due to the local steam supply when converting CO_2 to CO internally via RWGS. For PtMETH (Fig. 8 a), both CO and CO_2 methanation reactions are very exothermic, whose heat is enough to drive the steam generation for the chosen stack operating points. The minimal electrical heating is used only for heating the SOE inlets to 750 °C. Therefore, no big benefits could be offered by CE for producing methane without utilizing available waste heat.

For PtMeOH/DME (Fig. 8 b and c), CE significantly improves plant-wise heat integration, due to that (1) CE requires only half of the steam required by SE for the chosen operating points. (2) CO methanolization (Eq. (5)) is more exothermic than CO_2 methanolization (Eq. (4)). For the same amount of carbon conversion (without utilizing water condensation heat), CO methanolization generates 3.8 times more heat than CO_2 methanolization at 260 °C, while CO methanation generates only 1.3 times more heat compared to the CO_2 methanation at 300 °C. This is the major reason for the two different plateaus at 260 °C in Fig. 8 b and c. These two factors result in a significant reduction in electrical heating for CE compared with SE.

PtDME with SE (Fig. 8 c) needs more electrical heating than PtMeOH with SE, although a further exothermic DME synthesis step is introduced. This is due to that the employed methanol-to-DME process is operated with pressurized columns at 20 bar, which thus requires heat for re-boiling at 210 °C and worsens the heat integration.

For PtGASO, no big improvement of heat integration is contributed by CE, after introducing a further exothermic gasoline-synthesis process. The heat available from gasoline synthesis compensates the electrical heating of PtMeOH. There is still (waste) heat available to further enhance the overall efficiency of PtGASO.

4.2.2.2. System efficiency. The system efficiency of power-to-fuels depends mainly on four factors: (1) the operating point of the employed electrolyzer, (2) exergy destruction due to chemical reaction, (3) system-level heat integration, and (4) waste heat recovery. When comparing system performances of two SOE-based systems, similar operating points should be chosen, since the stack dominates the total power consumption and its operating points determine the electrolysis (electrical) efficiency, thus the overall efficiency [9]. Particularly, the stack temperature level affects

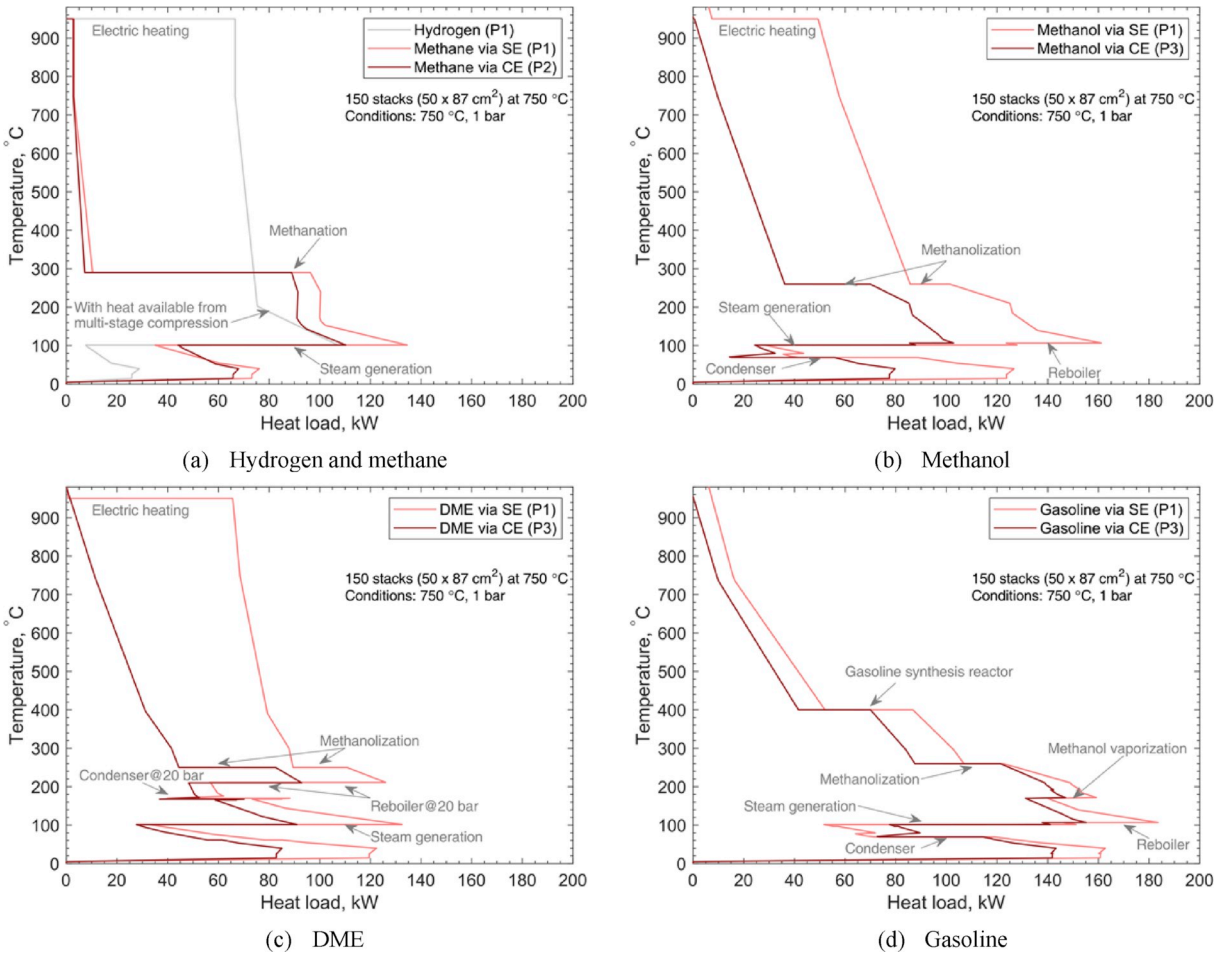

Fig. 8. Grand composite curves illustrating system-level heat integration. Operating points P1–P3 of the SOE at 750 °C and 1 bar refer to Table 2. The minimum temperature differences are 20–30 °C for gas streams and 10 °C for liquid streams.

dramatically the electrical efficiency, thus it is not reasonable to compare two systems with SOE operating at, e.g., 750 and 850 °C. Since the operating points of the SOE chosen in this paper are similar to each other and the waste heat recovery has not been considered, the factors (2) and (3) differentiate the system performances.

The initial system efficiencies with the stack operated at 750 °C are calculated considering heat integration and compared in Fig. 9 (a). In general, the more chemical-reaction (energy conversion) steps involved and the more difficult the chemical reactions, the larger the exergy destructions will occur, thus leading to lower system efficiencies. Therefore, PtH offers the highest efficiency (94%), followed by PtMETH (83%), which is easier compared to power-to-liquids. PtMeOH and PtDME via MeOH have similar system efficiency (70–80%), due to similar fuel synthesis processes. PtGASO offers the lowest efficiency of 65% for the route of MeOH-DME-GASO.

The benefit of CE for improving system efficiency is illustrated in Fig. 9 (a). If fuel synthesis processes are exothermic enough to drive all steam generation without electrical heating, it is not recommended to use CE. For example, for PtMETH and PtGASO, which require almost no electrical heating with SE (Fig. 9 b), CE can even slightly reduce the system efficiency, due to higher voltage (Fig. 9 a). Otherwise, if a lot of electrical heating is needed with SE, e.g., PtMeOH and PtDME, CE can reduce dramatically the electrical heating by improved heat integration (Fig. 9 b) with an efficiency enhancement.

4.2.3. Economic performance

The economic assumptions are 20-year plant life, 8% interest rate, 8000 annual operating hours (AOHs), 48 000-h stack lifetime, 81.64 €/MWh electricity price (similar to German 2018 average for non-household uses [109], including taxes and green certificate), and 40 €/ton CO_2 purchase price. The uncertainty of these parameters is not investigated here. The stack lifetime of 48 000 h is below the lower bound mentioned by industrial experts (60 000 to 90 000 h in 2020 [110]). Therefore, 3 replacements of the SOE stacks are needed for annual 8000-h operation for 20 years. The capital investment of most equipment is based on the cost functions given in Ref. [52], while that of SOE stacks is estimated by Ref. [111].

The specific capital expenditure (CAPEX) reduces with an increased plant capacity, particularly, when the SOE power is below 10–20 MWe for PtG and 20–30 MWe for PtL (Fig. 10). For small scales, CAPEX is dominated by the components and auxiliaries in the fuel synthesis processes. With an increase in plant size, the specific CAPEX of these components is reduced significantly due to the good economic scaling. When the plant scale is big enough, SOE dominates the specific CAPEX by 65–75% for PtL and over 80% for PtG. Additionally, at the same scale, the specific CAPEX of the CE plants is higher for PtMETH and PtGASO, but similar for PtMeOH and PtDME. This is mainly due to that (1) for the chosen operating points CE plants require more stacks to reach the same power scale, resulting in a higher specific SOE CAPEX of CE; and (2) for the same power scale, the mass production of MeOH and DME is higher than those of H_2, METH and GASO. As given in Fig. 10 a, the specific CAPEXs (€/kW LHV product) of the plants over 20 MWe are calculated as 2000–2500 for H_2, 2500–3000 (SE) and 3000–3500 (CE) for METH, 3500–4300 for MeOH, 3000–4000 for DME, 3800–5000 (SE) and 4000–5500 (CE) for GASO.

A similar trend of levelized cost of product (LCO) has been given in

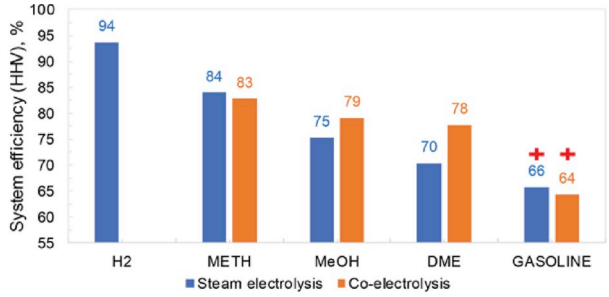

(a) HHV system efficiency for the considered process alternatives, with LHV efficiency given in SI. The red cross stands for the possibility of a further efficiency increase by using waste heat available.

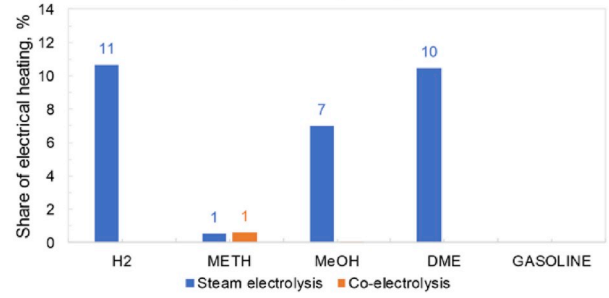

(b) Contribution of electrical heating to the total power consumption

Fig. 9. Comparison of thermodynamic performances of the power-to-fuel systems using the operating points of the SOE at 750 °C and 1 bar in Table 2. The given efficiencies are achieved without end-of-pipe waste heat utilization. Additional information, e.g., LHV efficiency, power consumption and product yield, is given in Figure S 12.

Fig. 10 (b); however, the LCO is stabilized with an SOE power over 5–10 MWe and there is no big difference between SE and CE plants for MeOH, DME (Fig. 10 b): 4.5–4.8 €/kg for H_2, 2.1–2.6 €/kg for METH, 1.0–1.1 €/kg for MeOH, 1.4–1.7 €/kg for DME, and 2.6–3.0 €/kg for GASO. Below 5 MWe, the impact of CAPEX on LCO is significant, while above 10 MWe the CAPEX share reduces to 30% and LCO is dominated by electricity consumption (over 60%).

Cheap or even free electricity, e.g., excess renewable power, can reduce the LCO; however, the decrease in the AOHs when using excess power can, on the contrary, increase the LCO. As shown in Fig. 11, if

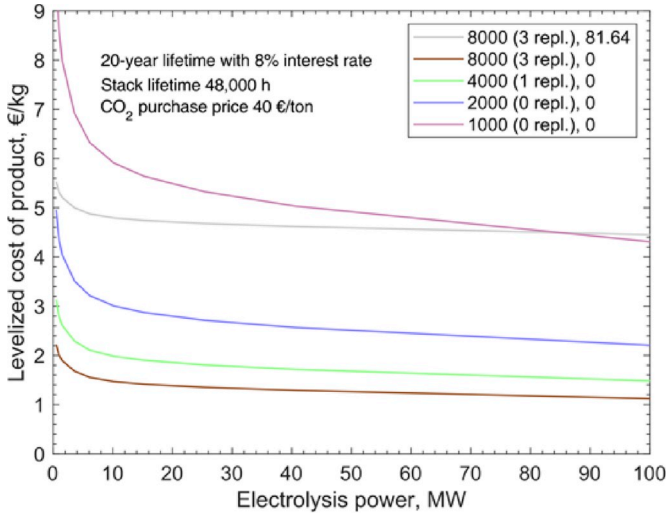

Fig. 11. Impacts of electricity price (0 or 81.64 €/MWh) and AOHs (1000–8000 h) on the LCO of H_2. Different AOHs vary the numbers of stack replacement (repl.) from 0 to 3 times. The costs for startup, shutdown, transition and product storage are not considered. The same information is available for each fuel in Figure S 14.

free electricity is available to drive the PtH system at full load for 8000 h per year, the LCO of H_2 which is dominated by the SOE CAPEX will be reduced by 70–75% to 1.2–1.4 €/kg; unfortunately, such an extreme case can hardly happen in reality. However, if the AOHs are reduced to 4000 (or 2000) with free electricity, interestingly, the LCO of H_2 is only increased by 30% (or 100%) compared to 8000 AOHs with free electricity. This is due to fewer stack replacements: only one replacement is needed for 4000 AOHs and no replacement required for 2000 AOHs. The decrease in the SOE CAPEX compensates, to some extent, the negative effect of the decrease in AOHs. Particularly, low electricity prices will amplify the contribution of SOE CAPEX to the LCO and will be more beneficial with a further reduction of SOE costs. If the AOHs are reduced from 2000 to only 1000 without a further reduced SOE CAPEX, there will be a significant increase in the LCO of H_2.

A similar trend is observed for all other fuels as shown in Figure S 14. It can be concluded that if free excess power is available for over 2000 h per year, the LCO of products can be even lower than 8000

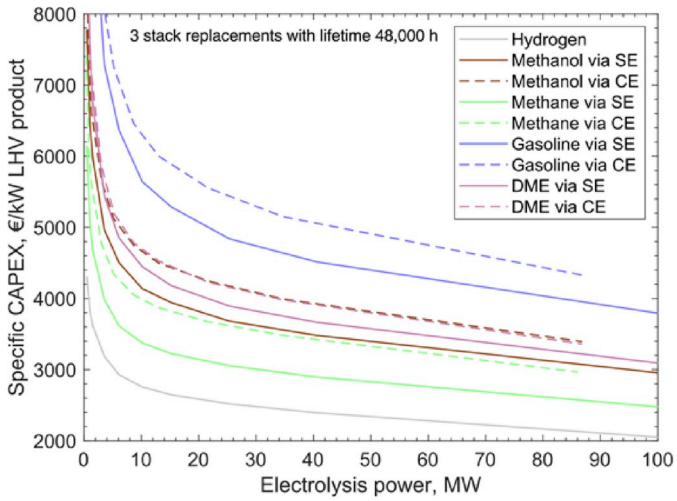

(a) CAPEX per kW product (LHV)

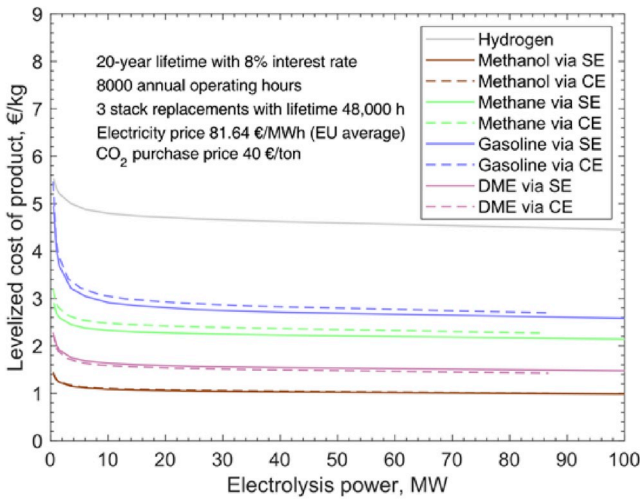

(b) Levelized cost of various products

Fig. 10. Economic indicators varied with plant scales (economic assumptions: 20-year plant lifetime with 8% interest rate, 8000 annual operating hours, 48 000-h stack lifetime, 81.64 €/MWh electricity price, and 40 €/ton CO_2 purchase price). Additional economic indicators are given in Figure S 13. The costs for startup, shutdown, transition and product storage (depending on use scenarios) are not considered.

AOHs with grid electricity price (81.64 €/MWh considered here), although still higher than industrial production prices. One may question whether it is possible to find a continuous supply of free electricity for several hours or even a day. The answer seems to be 'yes': based on the observed hours with negative electricity in Germany (with a relatively low renewable-energy share in its energy mix), the hours of negative prices are estimated to be over 1000–1800 h in 2030 [112]. More importantly, it has been reported that, during the first 10 months of 2017, negative prices of electricity occurred 103 times with a maximum period of 21 h [113]. Particularly, the prices in Germany at the day-ahead market of the EPEX Spot were below 0 €/MWh for a total of 31 h during 28–29 Sep 2017 with the lowest price of −83.06 €/MWh for 15 h [113]. A negative electricity price will further reduce the LCO.

4.3. Long-term operating strategy

Assuming constant current density and feed flows, stack degradation leads to an increase in voltage, which increases the SOE outlet temperature. If the degradation rate is relatively large, e.g., 17 mV/kh as measured for the tested stack (2014-design) [46], the SOE outlet temperature of PtMETH designed with P2 (Table 2) will reach 870 °C (1.39 V) after 10 kh operation with an efficiency drop from 83% down to 79% (Figure S 15 a); while, with a 5 mV/kh degradation, the SOE outlet temperature will reach 870 °C after 43 kh (Figure S 15b). It may be true that SOE lifetime in practice will be defined by the maximum allowed temperature of the stack and BoP but not by the operating voltage.

The stack cooling can only be offered by the feed flows. Increasing sweep-gas and/or steam feed flowrates can reduce the temperature gradient inside the stack. However, for a system with a specific design point, the steam flowrate can not be increased infinitely, due to that additional steam fed than the design amount worsens the heat integration and may require an extra electrical steam generator, thus reducing the system efficiency (Figure S 16 a, b). The only remaining effective means is thus increasing sweep-gas flowrate: With 20 sccm/cm^2 oxygen feed instead of 3 sccm/cm^2, the SOE lifetime can be significantly increased by 6 kh, although at the cost of lowering the system efficiency (Figure S 15 a).

Another way of controlling the stack temperature is to reduce the current density, so that less heat is produced internally. Thus, two temperature-control strategies were investigated assuming a constant degradation rate of 17 mV/kh (Fig. 12):

(i) S1: Set inlet and outlet temperatures equal along with the stack operation. Reduce the current density when needed to remain below 870 °C.
(ii) S2: Set inlet and outlet temperatures equal below 870 °C. Once over 870 °C, the inlet temperature is reset to 750 °C.

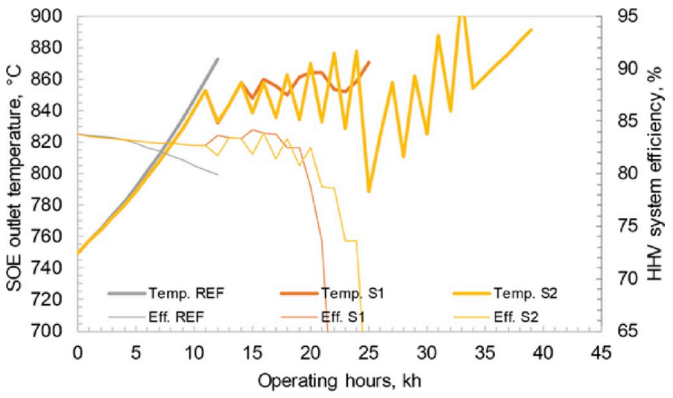

Fig. 12. Predicted SOE outlet temperature and system efficiency (HHV) along with operation with a constant degradation rate of 17 mV/kh. Reference (REF) case: SOE inlet temperature kept at 750 °C. No heat losses are considered. The step of current-density reduction is 0.05 A/cm^2 and can be smaller in practice. Additional information is available in Figure S 16.

For the first 10 kh with 0.5 A/cm^2, the SOE outlet temperatures of S1 and S2 are similar to the reference (REF), where the SOE inlet temperature is kept constant at 750 °C. System efficiencies of S1 and S2 are higher, due to the increased inlet temperature and the reduced voltage. The efficiencies are constant, due to that the temperature increase compensates the voltage increment from degradation. The electrical heating of S1 and S2 is kept constant, since the upper terminal temperature difference of the cathode-side heat exchanger can be considered as constant and electrical heater addresses fixed temperature increase of constant flowrates.

Between 10 and 20 kh, a decrease in the current density becomes necessary to maintain the cell temperature below 870 °C. A slight difference is observed between S1 and S2: The efficiency from S1 remains higher all the time, due to high cell temperature and low voltage (Figure S 16 a). Although the electrical heating is reduced for S2 (Figure S 16b), it can not compensate for the increase in electricity consumption due to a higher voltage (Figure S 16 a).

After 20 kh, big efficiency drops are found for both strategies, since the decreased current density reduces steam utilization and there is not enough heat from the system to vaporize all steam feed at 0.3 A/cm^2. A further decrease in the current density largely increases the electricity consumed by steam generation (Figure S 16b).

Therefore, the strategy S1 is preferred because (1) it reduces the temperature gradient between stack inlet and outlet at each time, and (2) it offers a higher system efficiency.

5. Conclusions

This paper investigated the SOE-based power-to-fuel systems from the levels of both stack and system. Three major original tasks have been performed: (1) at the stack level, practical operating windows were established with calibrated multi-physical stack model to support feasible stack operating points; (2) at the system level, techno-economic performances of power-to-hydrogen, -methane, -methanol, -dimethyl ether and -gasoline were compared comprehensively considering plant-wise heat integration with similar stack operating points; and (3) two long-term operating strategies were investigated to cope with the thermal management issue raised by stack degradation. The major original conclusions are:

- For stack operating windows, the temperature and electrochemical performance of the stack interact strongly under adiabatic conditions. Considering practical constraints, operating windows of the stack at 750 °C are relatively narrow at low current densities (below 0.4–0.5 A/cm^2) and enlarged at increased current densities (0.5–1.0 A/cm^2). Co-electrolysis and an increased sweep-gas flow can widen the operating windows.
- For thermodynamic performance, system efficiency of power-to-fuels depends on the chemical reaction process and plant-wise heat integration. With the stack operating at 750 °C, power-to-hydrogen achieves the highest efficiency (~95%, higher heating value), followed by power-to-methane (~83%), power-to-methanol/- dimethyl ether (70–80%) and power-to-gasoline (~65%). Co-electrolysis can improve the system efficiency of power-to-methanol/-dimethyl ether with less exothermic fuel-synthesis processes but offers no advantages in power-to-methane and -gasoline scenarios.
- For economic performance, the levelized cost of the final product of power-to-fuels is dominated by the electrical grid, if used as a single power source. The total capital investment is dominated by the stacks. With excess renewable electricity with low- or even -negative price, it is still possible to have competitive levelized costs with over 1000 annual operating hours, due to fewer stack replacements.

- For long-term operating strategy, the stack lifetime may be determined by the maximum allowed temperature but not the operating voltage. Increasing steam flowrate is not a feasible way to hinder the rise of stack temperature, as it only has a limited effect and may significantly worsen plant-wise heat integration. The increase in sweep-gas flowrate, although negatively affecting system efficiency, can be effective for controlling the stack temperature. It is recommended to increase the stack inlet temperature and keep this temperature close to the outlet temperature during operation.

Acknowledgement

This projects leading to these results have received funding from the Fuel Cells and Hydrogen Joint Undertaking under grant agreement No 699892 (ECo), 731224 (BALANCE) and 731125 (PENTAGON). This Joint Undertaking receives support from the European Union's Horizon 2020 research and innovation programme, Hydrogen Europe and Hydrogen Europe research. T.- E. Lin thanks the Young Scholar Fellowship Program by Ministry of Science and Technology (MOST) in Republic of China, under Grant MOST 108-2636-E-009-012.

Appendix A. Supplementary data

Supplementary data to this article can be found online at https://doi.org/10.1016/j.rser.2019.04.071.

Nomenclature

AOHs	Annual operating hours
BoP	Balance of plant
CAPEX	Capital expenditure
CE	Co-electrolysis
DME	Dimethyl ether
GASO	Gasoline
HHV	Higher heating value
LCO	Levelized cost of product
LHV	Lower heating value
LPG	Liquified petroleum gas
MeOH	Methanol
METH	Methane
MtG	Methanol-to-gasoline
OPEX	Operational expenditure
PtDME	Power-to-DME
PtG	Power-to-gas
PtGASO	Power-to-gasoline
PtH	Power-to-hydrogen
PtL	Power-to-liquid
PtMeOH	Power-to-methanol
PtMETH	Power-to-methane
RWGS	Reverse water-gas shift reaction
SE	Steam-electrolysis
SOE	Solid-oxide electrolyzer/electrolysis
SRU	Serial repeating unit
YSZ	Yttria stabilized zirconia

References

[1] Ebbesen SD, Jensen SH, Hauch A, Mogensen MB. High temperature electrolysis in alkaline cells, solid proton conducting cells, and solid oxide cells. Chem Rev 2014;114(21):10697–734.
[2] Fu Q, Mabilat C, Zahid M, Brisse A, Gautier L. Syngas production via high-temperature steam/CO 2 co-electrolysis: an economic assessment. Energy Environ Sci 2010;3(10):1382–97.
[3] Jensen SH, Graves C, Mogensen M, Wendel C, Braun R, Hughes G, Gao Z, Barnett SA. Large-scale electricity storage utilizing reversible solid oxide cells combined with underground storage of CO2 and CH4. Energy Environ Sci 2015;8(8):2471–9.
[4] Baldi F, Wang L, Pérez-Fortes M, Marechal F. A cogeneration system based on solid oxide and proton exchange membrane fuel cells with hybrid storage for off-grid applications. Frontiers in Energy Research 2018;6:139.
[5] Graves C, Ebbesen SD, Mogensen M, Lackner KS. Sustainable hydrocarbon fuels by recycling CO2 and H2O with renewable or nuclear energy. Renew Sustain Energy Rev 2011;15(1):1–23.
[6] Mougin J, Di Iorio S, Chatroux A, Donnier-Marechal T, Palcoux G, Petitjean M, Roux G. Development of a solid oxide electrolysis stack able to operate at high steam conversion rate and integration into a SOE system. vol. 78. ECS Transactions; 2017. p. 3065–75. 1.
[7] Li Q, Zheng Y, Guan W, Jin L, Xu C, Wang WG. Achieving high-efficiency hydrogen production using planar solid-oxide electrolysis stacks. Int J Hydrogen Energy 2014;39(21):10833–42.
[8] AlZahrani AA, Dincer I. Modeling and performance optimization of a solid oxide electrolysis system for hydrogen production. Appl Energy 2018;225:471–85.
[9] Wang L, Pérez-Fortes M, Madi H, Diethelm S, Maréchal F. Optimal design of solid-oxide electrolyzer based power-to-methane systems: a comprehensive comparison between steam electrolysis and co-electrolysis. Appl Energy 2018;211:1060–79.
[10] Peters R, Deja R, Blum L, Nguyen VN, Fang Q, Stolten D. Influence of operating parameters on overall system efficiencies using solid oxide electrolysis technology. Int J Hydrogen Energy 2015;40(22):7103–13.
[11] Mermelstein J, Posdziech O. Development and demonstration of a novel reversible SOFC system for utility and micro grid energy storage. Fuel Cells 2017;17(4):562–70.
[12] Bailera M, Lisbona P, Romeo LM, Espatolero S. Power to Gas projects review: lab, pilot and demo plants for storing renewable energy and CO2. Renew Sustain Energy Rev 2017;69:292–312.
[13] Sanz-Bermejo J, Muñoz-Antón J, Gonzalez-Aguilar J, Romero M. Part load operation of a solid oxide electrolysis system for integration with renewable energy sources. Int J Hydrogen Energy 2015;40(26):8291–303.
[14] Küngas R, Blennow P, Heiredal-Clausen T, Holt T, Rass-Hansen J, Primdahl S, Hansen JB. eCOs-a commercial CO2 electrolysis system developed by haldor Topsoe. ECS Transactions 2017;78(1):2879–84.
[15] Hansen JB. Solid oxide electrolysis–a key enabling technology for sustainable energy scenarios. Faraday Discuss 2015;182:9–48.
[16] Strohbach T, Mittmann F, Walter C, Schimanke D, Geipel C. Sunfire industrial SOC stacks and modules. ECS Transactions 2015;68(1):125–9.
[17] Zheng Y, Wang J, Yu B, Zhang W, Chen J, Qiao J, Zhang J. A review of high temperature co-electrolysis of H 2 O and CO 2 to produce sustainable fuels using solid oxide electrolysis cells (SOECs): advanced materials and technology. Chem Soc Rev 2017;46(5):1427–63.
[18] Nakajo A, Cocco AP, DeGostin MB, Peracchio AA, Cassenti BN, Cantoni M, Chiu WKS. Accessible triple-phase boundary length: a performance metric to account for transport pathways in heterogeneous electrochemical materials. J Power Sources 2016;325:786–800.
[19] Nakajo A, Kiss AM, Cocco AP, Harris WM, DeGostin MB, Greco F, Nelson GJ, Peracchio AA, Cassenti BN, Deriy A, Wang S. Characterization of cracks and their effects on the effective transport pathways in Ni-YSZ anodes after reoxidation using X-ray nanotomography. ECS Transactions 2015;68(1):1069–81.
[20] Cocco AP, Nelson GJ, Harris WM, Nakajo A, Myles TD, Kiss AM, Lombardo JJ, Chiu WK. Three-dimensional microstructural imaging methods for energy materials. Phys Chem Chem Phys 2013;15(39):16377–407.
[21] Schefold J, Brisse A, Poepke H. 23,000 h steam electrolysis with an electrolyte supported solid oxide cell. Int J Hydrogen Energy 2017;42(19):13415–26.
[22] Lin J, Chen L, Liu T, Xia C, Chen C, Zhan Z. The beneficial effects of straight open large pores in the support on steam electrolysis performance of electrode-supported solid oxide electrolysis cell. J Power Sources 2018;374:175–80.
[23] Zhang X, O'Brien JE, O'Brien RC, Hartvigsen JJ, Tao G, Housley GK. Improved durability of SOEC stacks for high temperature electrolysis. Int J Hydrogen Energy 2013;38(1):20–8.
[24] Nakajo A, Mueller F, Brouwer J, Favrat D. Progressive activation of degradation processes in solid oxide fuel cells stacks: Part I: lifetime extension by optimisation of the operating conditions. J Power Sources 2012;216:449–63.
[25] Hubert M, Laurencin J, Cloetens P, Da Silva JC, Lefebvre-Joud F, Bleuet P, Nakajo A, Siebert E. Role of microstructure on electrode operating mechanisms for mixed ionic electronic conductors: from synchrotron-based 3D reconstruction to electrochemical modeling. Solid State Ionics 2016;294:90–107.
[26] Hauth M, Lawlor V, Cartellieri P, Zechmeister C, Wolff S, Bucher C, Malzbender J, Wei J, Weber A, Tsotridis G, Frandsen HL. Production and reliability oriented SOFC cell and stack design. ECS Transactions 2017;78(1):2231–49.
[27] HELMETH. European. Union's Seventh Framework Programme (FP7/2007-2013) for the fuel cells and hydrogen joint technology initiative: integrated high-temperature electrolysis and methanation for effective power to gas conversion accessed http://www.helmeth.eu, Accessed date: 2 April 2017.
[28] Jeanmonod G, Wang L, Diethelm S, Maréchal F, Van herle J. Trade-off designs of power-to-methane systems via solid-oxide electrolyzer and the application to biogas upgrading. Appl Energy 2019;247:572–81.
[29] www.pentagon-project.eu/.
[30] Wang L, Düll J, Maréchal F, Van herle J. Trade-off designs and comparative exergy evaluation of solid-oxide electrolyzer based power-to-methane plants. Int J Hydrogen Energy 2019;44:9529–43.
[31] European Union Horizon 2020 project GrInHy, green industrial hydrogen via reversible high-temperature electrolysis. www.green-industrial-hydrogen.com/home/.
[32] Giglio E, Deorsola FA, Gruber M, Harth SR, Morosanu EA, Trimis D, Bensaid S, Pirone R. Power-to-gas through high temperature electrolysis and carbon dioxide methanation: reactor design and process modeling. Ind Eng Chem Res 2018;57(11):4007–18.

[33] Wagner PH. Integrated design, optimization, and experimental realization of a steam-driven micro recirculation fan for solid oxide fuel cell systems EPFL; 2019. PhD. THESIS.
[34] Stoots C, O'Brien J, Hartvigsen J. Results of recent high temperature coelectrolysis studies at the Idaho National Laboratory. Int J Hydrogen Energy 2009;34(9):4208–15.
[35] Diethelm S, herle JV, Montinaro D, Bucheli O. Electrolysis and Co-electrolysis performance of SOE short stacks. Fuel Cells 2013;13(4):631–7.
[36] Schefold J, Brisse A, Zahid M. Long term testing of solid oxide fuel cell stacks with yttria stabilized zirconia electrolyte in the H2O electrolysis mode. ECS Transactions 2010;28(11):357–67.
[37] Stoots CM, O'Brien JE, Condie KG, Hartvigsen JJ. High-temperature electrolysis for large-scale hydrogen production from nuclear energy–experimental investigations. Int J Hydrogen Energy 2010;35(10):4861–70.
[38] Zheng Y, Li Q, Guan W, Xu C, Wu W, Wang WG. Investigation of 30-cell solid oxide electrolyzer stack modules for hydrogen production. Ceram Int 2014;40(4):5801–9.
[39] Schefold J, Brisse A, Zahid M, Ouweltjes JP, Nielsen JU. Long term testing of short stacks with solid oxide cells for water electrolysis. ECS Transactions 2011;35(1):2915–27.
[40] Ebbesen SD, Høgh J, Nielsen KA, Nielsen JU, Mogensen M. Durable SOC stacks for production of hydrogen and synthesis gas by high temperature electrolysis. Int J Hydrogen Energy 2011;36(13):7363–73.
[41] Chen M, Høgh JVT, Nielsen JU, Bentzen JJ, Ebbesen SD, Hendriksen PV. High temperature Co-electrolysis of steam and CO2 in an SOC stack: performance and durability. Fuel Cells 2013;13(4):638–45.
[42] Corre G, Brisse A. 9000 hours operation of a 25 solid oxide cells stack in steam electrolysis mode. ECS Transactions 2015;68(1):3481–90.
[43] Fang Q, Blum L, Menzler NH. Performance and degradation of solid oxide electrolysis cells in stack. J Electrochem Soc 2015;162(8):F907–12.
[44] Kotisaari M, Thomann O, Montinaro D, Kiviaho J. Evaluation of a SOE stack for hydrogen and syngas production: a performance and durability analysis. Fuel Cells 2017;17(4):571–80.
[45] Rinaldi G, Diethelm S, Oveisi E, Burdet P, Van Herle J, Montinaro D, Fu Q, Brisse A. Post-test analysis on a solid oxide cell stack operated for 10,700 hours in steam electrolysis mode. Fuel Cells 2017;17(4):541–9.
[46] Agersted K, Chen M, Blennow P, Küngas R, Vang Hendriksen P. Long-term operation of a solid oxide cell stack for co-electrolysis of steam and CO2 [Chapter 06] - Sessions B05, A08, A11 - 205/337. *12th european SOFC & SOE forum*, 5 - 8 july 2016. Switzerland: Lucerne; 2016.
[47] Hjalmarsson P, Sun X, Liu YL, Chen M. Influence of the oxygen electrode and inter-diffusion barrier on the degradation of solid oxide electrolysis cells. J Power Sources 2013;223:349–57.
[48] Sun X, Chen M, Hendriksen PV, Mogensen MB. Durable solid oxide electrolysis cells for hydrogen production. B1305 in 11th european SOFC & SOE forum. Switzerland: Lucerne; 2014.
[49] Küngas Rainer, Peter Blennow, Heiredal-Clausen Thomas, Nørby Tobias Holt, Rass-Hansen Jeppe. Poul Georg Moses. Increasing the lifetime of stacks in CO2 electrolysis. *Proceedings of the 13th european SOFC & SOE forum.* 2018. p. B1503.
[50] Küngas R, Blennow P, Heiredal-Clausen T, Holt T, Rass-Hansen J, Primdahl S. Systematic lifetime testing of stacks in CO2 electrolysis. ECS Transactions 2017;78(1):2895–905.
[51] Rao M, Sun X, Hagen A. Long term testing of solid oxide electrolysis cells under Co-electrolysis conditions. ECS Transactions 2017;80(9):57–69. https://doi.org/10.1149/08009.0057ecst.
[52] Turton R, Bailie RC, Whiting WB, Shaeiwitz JA. Analysis, synthesis and design of chemical processes. Pearson Education; 2008.
[53] Gao J, Wang Y, Ping Y, Hu D, Xu G, Gu F, Su F. A thermodynamic analysis of methanation reactions of carbon oxides for the production of synthetic natural gas. RSC Adv 2012;2(6):2358–68.
[54] Schaaf T, Grünig J, Schuster MR, Rothenfluh T, Orth A. Methanation of CO2-storage of renewable energy in a gas distribution system. Energy, Sustainability and Society 2014;4(1):2.
[55] Rönsch S, Schneider J, Matthischke S, Schlüter M, Götz M, Lefebvre J, Prabhakaran P, Bajohr S. Review on methanation–From fundamentals to current projects. Fuel 2016;166:276–96.
[56] Gao J, Liu Q, Gu F, Liu B, Zhong Z, Su F. Recent advances in methanation catalysts for the production of synthetic natural gas. RSC Adv 2015;5(29):22759–76.
[57] Zhao K, Wang L, Calizzi M, Moioli E, Züttel A. In situ control of the adsorption species in CO2 hydrogenation: determination of intermediates and byproducts. J Phys Chem C 2018;122(36):20888–93.
[58] Zhao, K.; Wang, L.; Moioli, E.; Calizzi, M. and Züttel, A. Identifying reaction species by evolutionary fitting and kinetic analysis: an example of CO2 hydrogenation in DRIFTS. J Phys Chem C, DOI: 10.1021/acs.jpcc.8b11105.
[59] Jalama K. Carbon dioxide hydrogenation over nickel-, ruthenium-, and copper-based catalysts: review of kinetics and mechanism. Catal Rev 2017;59(2):95–164.
[60] Wang W, Wang S, Ma X, Gong J. Recent advances in catalytic hydrogenation of carbon dioxide. Chem Soc Rev 2011;40(7):3703–27.
[61] Gallandat N, Mutschler R, Vernay V, Yang H, Züttel A. Experimental performance investigation of a 2 kW methanation reactor. Sustainable Energy & Fuels 2018;2(5):1101–10.
[62] Moioli E, Mutschler R, Züttel A. Renewable energy storage via CO2 and H2 conversion to methane and methanol: assessment for small scale applications. Renew Sustain Energy Rev 2019;107:497–506.
[63] Götz M, Lefebvre J, Mörs F, Koch AM, Graf F, Bajohr S, Reimert R, Kolb T. Renewable Power-to-Gas: a technological and economic review. Renew Energy 2016;85:1371–90.
[64] Schlereth D, Hinrichsen O. A fixed-bed reactor modeling study on the methanation of CO2. Chem Eng Res Des 2014;92(4):702–12.
[65] Er-Rbib H, Bouallou C. Modeling and simulation of CO methanation process for renewable electricity storage. Energy 2014;75:81–8.
[66] Kangas P, Vázquez FV, Savolainen J, Pajarre R, Koukkari P. Thermodynamic modelling of the methanation process with affinity constraints. Fuel 2017;197:217–25.
[67] Kiewidt L, Thöming J. Predicting optimal temperature profiles in single-stage fixed-bed reactors for CO2-methanation. Chem Eng Sci 2015;132:59–71.
[68] Wang L, Rao M, Diethelm S, Lin T-E, Zhang H, Hagen A, Maréchal F, Van herle J. Power-to-methane via co-electrolysis of H2O and CO2: The effects of pressurized operation and internal methanation. Applied Energy; 2019. [revision submitted].
[69] Biedermann P, Grube T, Höhlein B. Methanol as an energy carrier. Zentralbibliothek: Forschungszentrum Jülich; 2006.
[70] Basu S, Khan AL, Cano-Odena A, Liu C, Vankelecom IF. Membrane-based technologies for biogas separations. Chem Soc Rev 2010;39(2):750–68.
[71] Ertl G, Knözinger H, Weitkamp J, editors. Handbook of heterogeneous catalysis. 1997.
[72] Van-Dal ÉS, Bouallou C. Design and simulation of a methanol production plant from CO2 hydrogenation. J Clean Prod 2013;57:38–45.
[73] Ebbesen SD, Graves C, Mogensen M. Production of synthetic fuels by co-electrolysis of steam and carbon dioxide. Int J Green Energy 2009;6(6):646–60.
[74] Pontzen F, Liebner W, Gronemann V, Rothaemel M, Ahlers B. CO2-based methanol and DME–Efficient technologies for industrial scale production. Catal Today 2011;171(1):242–50.
[75] Manenti F, Cieri S, Restelli M, Bozzano G. Dynamic modeling of the methanol synthesis fixed-bed reactor. Comput Chem Eng 2013;48:325–34.
[76] Manenti F, Cieri S, Restelli M. Considerations on the steady-state modeling of methanol synthesis fixed-bed reactor. Chem Eng Sci 2011;66(2):152–62.
[77] Abrol S, Hilton CM. Modeling, simulation and advanced control of methanol production from variable synthesis gas feed. Comput Chem Eng 2012;40:117–31.
[78] Milani D, Khalilpour R, Zahedi G, Abbas A. A model-based analysis of CO2 utilization in methanol synthesis plant. Journal of CO2 Utilization 2015;10:12–22.
[79] Park N, Park MJ, Ha KS, Lee YJ, Jun KW. Modeling and analysis of a methanol synthesis process using a mixed reforming reactor: perspective on methanol production and CO2 utilization. Fuel 2014;129:163–72.
[80] Van-Dal ÉS, Bouallou C. Design and simulation of a methanol production plant from CO2 hydrogenation. J Clean Prod 2013;57:38–45.
[81] Ullmann F, Gerhartz W, Yamamoto YS, Campbell FT, Pfefferkorn R, Rounsaville JF. Ullmann's encyclopedia of industrial chemistry. VCH publishers; 1985.
[82] Pérez-Fortes M, Schöneberger JC, Boulamanti A, Tzimas E. Methanol synthesis using captured CO2 as raw material: techno-economic and environmental assessment. Appl Energy 2016;161:718–32.
[83] Asif M, Gao X, Lv H, Xi X, Dong P. Catalytic hydrogenation of CO2 from 600 MW supercritical coal power plant to produce methanol: a techno-economic analysis. Int J Hydrogen Energy 2018;43(5):2726–41.
[84] Tock L, Gassner M, Maréchal F. Thermochemical production of liquid fuels from biomass: thermo-economic modeling, process design and process integration analysis. Biomass Bioenergy 2010;34(12):1838–54.
[85] García-Trenco A, Martínez A. Direct synthesis of DME from syngas on hybrid CuZnAl/ZSM-5 catalysts: new insights into the role of zeolite acidity. Appl Catal Gen 2012;411:170–9.
[86] Flores JH, Peixoto DPB, Appel LG, De Avillez RR, da Silva MP. The influence of different methanol synthesis catalysts on direct synthesis of DME from syngas. Catal Today 2011;172(1):218–25.
[87] Naik SP, Ryu T, Bui V, Miller JD, Drinnan NB, Zmierczak W. Synthesis of DME from CO2/H2 gas mixture. Chem Eng J 2011;167(1):362–8.
[88] De Falco M, Capocelli M, Centi G. Dimethyl ether production from CO2 rich feedstocks in a one-step process: thermodynamic evaluation and reactor simulation. Chem Eng J 2016;294:400–9.
[89] Frusteri F, Cordaro M, Cannilla C, Bonura G. Multifunctionality of Cu–ZnO–ZrO2/H-ZSM5 catalysts for the one-step CO2-to-DME hydrogenation reaction. Appl Catal B Environ 2015;162:57–65.
[90] Frusteri F, Migliori M, Cannilla C, Frusteri L, Catizzone E, Aloise A, Giordano G, Bonura G. Direct CO2-to-DME hydrogenation reaction: new evidences of a superior behaviour of FER-based hybrid systems to obtain high DME yield. Journal of CO2 Utilization 2017;18:353–61.
[91] Bîldea CS, Győrgy R, Brunchi CC, Kiss AA. Optimal design of intensified processes for DME synthesis. Comput Chem Eng 2017;105:142–51.
[92] Ail SS, Dasappa S. Biomass to liquid transportation fuel via Fischer Tropsch synthesis–technology review and current scenario. Renew Sustain Energy Rev 2016;58:267–86.
[93] https://www.chemengonline.com/first-commercial-power-liquids-plant-planned/?printmode=1.
[94] https://www.sunfire.de/en/company/news/detail/first-commercial-plant-for-the-production-of-blue-crude-planned-in-norway?file=files/sunfire/images/content/company/press/2017_sunfire_PR_Nordic-Blue-Crude.pdf.
[95] www.topsoe.com/processes/gasoline-synthesis/gasoline-synthesis-tigas.
[96] https://blog.topsoe.com/2014/08/groundbreaking-turkmenistan-build-major-plant-producing-synthetic-gasoline.
[97] Sadeghi S, Haghighi M, Estifaee P. Methanol to clean gasoline over nanostructured CuO–ZnO/HZSM-5 catalyst: influence of conventional and ultrasound assisted co-impregnation synthesis on catalytic properties and performance. J Nat Gas Sci Eng 2015;24:302–10.
[98] Wan Z, Wu W, Li GK, Wang C, Yang H, Zhang D. Effect of SiO2/Al2O3 ratio on the

performance of nanocrystal ZSM-5 zeolite catalysts in methanol to gasoline conversion. Appl Catal Gen 2016;523:312–20.
[99] Meng F, Wang Y, Wang S. Methanol to gasoline over zeolite ZSM-5: improved catalyst performance by treatment with HF. RSC Adv 2016;6(63):58586–93.
[100] Wan Z, Wu W, Chen W, Yang H, Zhang D. Direct synthesis of hierarchical ZSM-5 zeolite and its performance in catalyzing methanol to gasoline conversion. Ind Eng Chem Res 2014;53(50):19471–8.
[101] Rajagopalan, S., Harandi, M.N. and Hickey, K.J., ExxonMobil Research and Engineering Co, 2018. Efficient process for converting methanol to gasoline. U.S. Patent Application 15/825,224.
[102] Joensen, F., Mentzel, U.V. and Menjon, I., Haldor Topsoe AS, 2018. Process for converting methanol to hydrocarbons suitable for use as gasoline or blendstock. U. S. Patent Application 15/544,670.
[103] Hannula I. Synthetic fuels and light olefins from biomass residues, carbon dioxide and electricity. Espoo: VTT. Julkaisu: VTT Science 2015;107.
[104] Marechal F, Kalitventzeff B. Targeting the integration of multi-period utility systems for site scale process integration. Appl Therm Eng 2003;23(14):1763–84.
[105] Gassner M, Maréchal F. Methodology for the optimal thermo-economic, multi-objective design of thermochemical fuel production from biomass. Comput Chem Eng 2009;33(3):769–81.
[106] Wang L, Yang Z, Sharma S, Mian A, Lin TE, Tsatsaronis G, Maréchal F, Yang Y. A review of evaluation, optimization and synthesis of energy systems: methodology and application to thermal power plants. Energies 2019;12(1):73.
[107] Navasa M, Graves C, Chatzichristodoulou C, Skafte TL, Sundén B, Frandsen HL. A three-dimensional multiphysics model of a solid oxide electrochemical cell: a tool for understanding degradation. Int J Hydrogen Energy 2018;43(27):11913–31.
[108] Stoots CM, O'Brien JE, Herring JS, Hartvigsen JJ. Idaho National Laboratory experimental research in high temperature electrolysis for hydrogen and syngas production (No. INL/CON-08-14622). Idaho National Laboratory (INL); 2008.
[109] [EUR_per_kWh).png] https://ec.europa.eu/eurostat/statistics-explained/index.php?title=File:Electricity_prices,_First_semester_of_2016-2018_.
[110] Schmidt O, Gambhir A, Staffell I, Hawkes A, Nelson J, Few S. Future cost and performance of water electrolysis: an expert elicitation study. Int J Hydrogen Energy 2017;42(52):30470–92.
[111] Jégoux M, de Saint Jean M, Wang L, Brunot A. Report on LCA and techno-economic analysis European Union; 2017. 2020 project SOPHIA deliverable 2.5.
[112] Nelson D, Huxham M, Muench S, O'Connell B. Policy and investment in German renewable energy. A CPI Report, Climate Policy Initiative. 2016.
[113] blog.energybrainpool.com/en/already-103-times-negative-electricity-prices-at-the-spot-market/; accessed on 17 Sep 2018.